Published online November 18, 2004

Nucleic Acids Research, 2004, Vol. 32, No. 20 ***6047–6056***
doi:10.1093/nar/gkh931

The stability of Seeman JX DNA topoisomers of paranemic crossover (PX) molecules as a function of crossover number

Prabal K. Maiti, Tod A. Pascal, Nagarajan Vaidehi and William A. Goddard III*

Materials and Process Simulation Center (MSC), MC 139-74, California Institute of Technology, Pasadena, CA 91125, USA

Received August 18, 2004; Revised and Accepted October 21, 2004

ABSTRACT

We use molecular dynamics simulations in explicit water and salt (Na^+) to determine the effect of varying the number of crossover points on the structure and stability of the PX65 paranemic crossover DNA molecule and its JXM topoisomers (M denotes the number of missing crossover points), recently synthesized by the Seeman group at New York University. We find that PX65, with six crossover points, is the most stable, and that the stability decreases monotonically with the number of crossover points PX65 > JX1 > JX2 > JX3 > JX4, with 6, 5, 4, 3 and 2 crossover points, respectively. Thus, for PX65/JX1, the strain energy is ~3 kcal/mol/bp, while it is ~13 kcal/mol/bp for JX2, JX3 and JX4. Another measure of the stability is the change in the structure from the minimum energy structure to the equilibrium structure at 300 K, denoted as root-mean-square deviation in coordinates (CRMSD). We find that CRMSD is ~3.5 Å for PX65, increases to 6 Å for JX1 and increases to 10 Å for JX2/JX3/JX4. As the number of crossover points decreases, the distance between the two double helical domains of the PX/JX molecules increases from ~20 Å for PX65 to 23 Å for JX4. This indicates that JX2, JX3 and JX4 are less likely to form, at least in with Na^+. However, in all the cases, the two double helical domains have average helicoidal parameters similar to a typical B-DNA of similar length and base sequence.

INTRODUCTION

DNA double helix structures are emerging as a useful scaffold for creating nanostructures and as components for nanomechanical devices (1,2). Self-assembly of various branched DNA motifs is emerging as an important route for constructing 2D and 3D periodic or aperiodic arrays (3–6), with potential application in DNA-based computation (7–9). Recently, Yan *et al.* (10) reported the construction of DNA-based nanogrids that provide an excellent scaffold for the production of highly conductive, uniform width silver nanowires. A variety of unusual DNA motifs has been synthesized for constructing nanomechanical devices (11–13). To facilitate the construction of robust DNA nanomechanical devices, the Seeman laboratory at New York University recently invented the new paranemic crossover (PX) class of DNA motifs (14,15) and their JXM topoisomers.

The PX DNA is a four-stranded molecule, in which two parallel double helices are joined by reciprocal exchange of strands at every point where the strands come together (15,16) (see Figure 2). The JXM structure is related to PX by containing M adjacent sites where backbones of the two parallel double helices *juxtapose without crossing over*. Seeman and co-workers (15) have demonstrated that interconversion between PX and JX2 states leads to robust DNA mechanical devices. However, no detailed structural characterizations have been made for these JXM molecules. Earlier, we demonstrated (Maiti,P.K., Pascal,T.A., Vaidehi,N., Heo,J. and Goddard,W.A.I., submitted) the use of molecular dynamics (MD) simulations to characterize the thermodynamic stability of PX motifs, where we found the PX65 DNA motif, to be particularly stable. This paper focuses on the JXM topoisomers related to PX65. To assess the relative stability of PX65 and its various JX isomers, we used MD to extract thermodynamic and structural parameters of these molecules as a function of the number of crossovers.

The PX65 molecule has six crossover points at positions 5, 11, 16, 22, 27 and 33, leading to the structure shown in Figure 1. Removing the middle crossover point (position 22) leads to the JX1 molecule (Figure 2). Similarly omitting two, three and four contiguous crossover points leads to the JX2, JX3 and JX4 motifs (also in Figure 2). The details of the MD simulation methods and of building the structures of the PX/JX motifs are given in Methods. The results from MD simulation on these DNA motifs are presented in Results and Discussion. The conclusions are in Summary and Conclusions.

METHODS

Building atomic-level PX nanostructures

The base pair sequences used for building the PX65/JXM molecules are shown in Figure 1. Each PX/JX structure

*To whom correspondence should be addressed. Tel: +1 626 395 2731; Email: wag@wag.caltech.edu
Present address:
Prabal K. Maiti, Department of Physics, Indian Institute of Science, Bangalore 560012, India

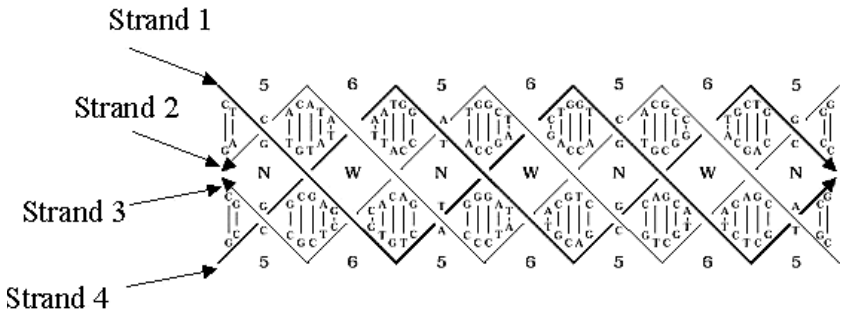

Strand 1: 5'-CTCTGTATAATGGAACCGACTGGTCTGCGGTGCTGGCC-3'
Strand 2: 3'-GAGACATATTACCTTGGCTGACCAGACGCCACGACCGG-5'
Strand 3: 5'-GCGGCGAGGTGTCTGGGATTGCAGGCAGCATCTCGACG-3'
Strand 4: 3'-CGCCGCTCCACAGACCCTAACGTCCGTCGTAGAGCTGC-5'

Figure 1. The base pair sequences used in the generations of PX65, JX1, JX2, JX3 and JX4 crossover molecules.

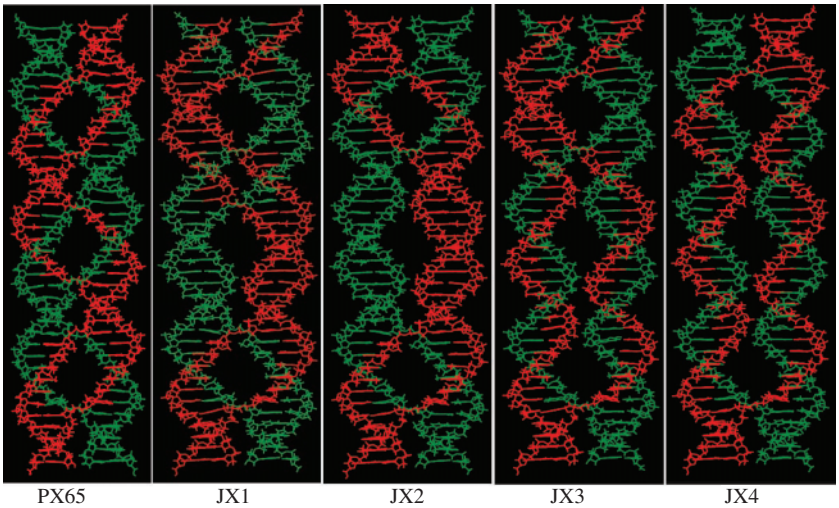

Figure 2. Generation of PX and JX DNA by reciprocal exchange. This illustrates the consequences of performing a crossover at various positions. PX65 has six crossover points. JX1, JX2, JX3 and JX4 have 5, 4, 3 and 2 crossover points, respectively.

has two double helical domains and has crossover points between strands of the same polarity. In the notation PXMN (say PX65), the first integer, $M = 6$, indicates the number of base pairs in the major groove; the second integer, $N = 5$, indicates the number in the minor groove. Thus, as shown in Figure 2, PX65 has two green strands and two red strands that intertwine each other with six crossover points. The five cases considered here (PX65, JX1, JX2, JX3 and JX4) all have 5 nucleotides in the minor groove and 6 nucleotides in the major groove.

The construction of these five PX/JX DNA motifs used the nucleic acid builder program Namot2 (17) (version 2.2.). The procedure for constructing these structures is as follows:

(i) *Building the DNA double helices*. First we create two regular B-DNA molecules, with the sequence given in Figure 1. Each of the double helices has 11 bp per turn. Table 1 shows the twist angles used for building the various PX/JX structures. We assigned the same twist angle for all the base pairs in the helical half turn. The helical rise value of 3.4 Å was used to build all the crossover structures.

(ii) *Building the crossover points*. When a double helix is built in Namot2, the molecules are oriented so that the 5′ and 3′ ends of the double helices are parallel to the y-axis. To create realistic crossover structures, it is necessary to rotate the individual helices so that the desired crossover points are closest to each other (rotation angles shown in Table 1). To find this point, we wrote a program that starts with the first crossover point and rotates the first helix in 1° increment to find the rotation leading to the shortest distance between these crossover points. Then the first helix is fixed at this prescribed value, while the second helix is rotated to achieve the shortest distance between the crossover points. The second helix is rotated 180° more than the first helix so that the helices are arranged as shown in Figure 2. The crossovers were then created using the 'nick' and 'link' commands in Namot2. These structures are saved in the PDB file format.

Table 1. Helical twist and rotation angles (in degrees) used in building various PX/JX starting structures

PX structure	Twist angle (degrees)	Base pairs per turn	Rotation angles° (about z-axis) Helix 1	Helix 2
PX65	30	11	60	240
JX1	30	11	60	240
JX2	30	11	60	240
JX3	30	11	60	240
JX4	30	11	60	240

Simulation details for the PX–JX structures

All MD simulations reported in this paper used the AMBER7 software package (18) with the all-atom AMBER95 force field (FF) (19). AMBER95 FF has been validated for MD simulations of B-DNA in explicit water with salt, starting from the crystal structure (20–24). These validation studies found that the CRMS deviation from the crystal structure for a dodecamer structure is typically <4 Å.

The electrostatics interactions were calculated with the Particle Mesh Ewald (PME) method (25,26) using a cubic B-spline interpolation of order 4 and a 10^{-4} tolerance set for the direct space sum cut-off. A real space cut-off of 9 Å was used both for the electrostatics and van der Waals interactions with a non-bond list update frequency of 10.

Using the LEAP module in AMBER, the PX/JX nanostructures were immersed in a water box using the TIP3P model for water. The box dimensions were chosen in order to ensure a 10 Å solvation shell around the DNA structure. In addition, some quantity of water was replaced by Na^+ counter ions to neutralize the negative charge on the phosphate groups of the backbone of the PX/JX structures. This procedure resulted in solvated structures, containing ~37 000 atoms. The solvated structures were then subjected to 1000 steps of steepest descent minimization of the potential energy, followed by 2000 steps of conjugate gradient minimization. During this minimization, the PX/JX DNA nanostructures were fixed in their starting conformations using harmonic constraints with a force constant of 500 kcal/mol/Å^2. This allowed the water molecules to reorganize to eliminate bad contacts with the PX structures.

The minimized structures were then subjected to 40 ps of MD, using a 2 fs time step for integration. During the MD, the system was gradually heated from 0 to 300 K using weak 20 kcal/mol/Å^2 harmonic constraints on the solute to its starting structure. This allows for slow relaxation of the built PX structures. In addition, SHAKE constraints (27) using a geometrical tolerance of 5×10^{-4} Å were imposed on all covalent bonds involving hydrogen atoms. This is needed to dynamically prevent changes in the NH and OH bonds from disrupting associated hydrogen bonds. Subsequently, MD was performed under constant pressure–constant temperature conditions (NPT), with temperature regulation achieved using the Berendsen weak coupling method (28) (0.5 ps time constant for heat bath coupling and 0.2 ps pressure relaxation time). This was followed by another 5000 steps of conjugate gradient minimization while decreasing the force constant of the harmonic restraints from 20 kcal/mol/Å^2 to zero in steps of 5 kcal/mol Å^2.

We then carried out 100 ps of unconstrained NPT MD to equilibrate the system at 300 K. We have found for other systems that the above equilibration protocol produces very stable MD trajectories for simulating large DNA nanostructures (Maiti,P.K., Pascal,T.A., Vaidehi,N., Heo,J. and Goddard,W.A.I., submitted). Finally, for analysis of structures and properties, we carried out 2 ns of NVT MD using a heat bath coupling time constant of 1 ps.

Methods used for calculating various properties of the PX nanostructures

Flexibility of the PX nanostructures from MD. To obtain the structure of each PX/JX nanostructures equilibrated in salt and water, we averaged the coordinates of each MD snapshot from 1 to 2 ns at 1 ps time intervals. This averaging was performed only for the last 1 ns to ensure that the structure had converged. This average structure represents the 'solution structure' of the PX/JX nanostructures.

Then, to obtain a measure of the flexibility of these structures, we calculated the root-mean-square deviation in coordinates, CRMSD, from the average solution structure for all atoms at each time step. This was performed at every 1 ps time interval in the final 1 ns of MD trajectory. This CRMSD is a measure of the overall flexibility of the PX/JX structures in solution. We also calculated the CRMSD for each base pair from the minimized starting structure using the time average over the last 200 ps for each base pair. This CRMSD from the minimized starting structure shows the flexibility of various regions of the PX/JX structure in solution.

Strain energy or the thermodynamic stability of the crossover motifs. To obtain a measure of the strain energy, we first partition the potential energy into a sum over atoms. This is performed by assigning half the energy for every two-body interaction to each of the two atoms, all the energy for each three-body interaction and each four-body inversion term to the central atom, and half the energy for every four-body dihedral (torsion) interaction to each of the two central atoms. Then, we collect these atomic energies together for each base of the DNA. Since the reference energy in the FF based simulations is not well defined, we use the reference energy for each base pair of the double helix formed by removing the crossover points between the double helices as a reference state. Then, for each base of the crossover nanostructures, we define the strain energy as the change from the reference structure. Then, summing over all bases, we obtain the total strain energy in each PX/JX structure, which we consider to determine the relative stability between the various crossover structures. Thus, the strain energy is defined as,

$$\Delta\Delta H^{\text{strain}}(\text{crossover structure}) = \Delta H(\text{crossover structure}) - 2\Delta H(\text{double helix}) \quad \mathbf{1}$$

where

(i) $\Delta\Delta H^{\text{strain}}$ is the sum of the strains in a given crossover nanostructure (PX/JX molecules),
(ii) ΔH(crossover structure) is the potential energy of the crossover structure (which is the sum of the strains),
(iii) ΔH(double helix) is the potential energy of the corresponding double helix without the crossover points (sum of the strains).

This strain energy represents the energy cost for making a crossover structure and does not include the dependence of the strain energy on the length of the PX/JX structures or the sequence. The average strain energy is calculated by averaging over 200 snapshots uniformly distributed over the last 200–400 ps of the 2 ns MD run. The strain energy per base pair is obtained by dividing the total strain energy from Equation 1 by the number of base pairs in each of the crossover structures. The experimental measure for stability is the melting temperature. This is straightforward to measure but difficult to calculate, since the final state of melting is not so well defined.

The vibrational density of states (DoS) of PX/JX DNA. We also calculated the vibrational DoS of PX/JX nanostructures from the MD as follows (29). First, we calculated the velocity auto-correlation function $C(t)$, defined as the mass weighted sum of the atom velocity autocorrelation functions

$$C(t) = \sum_{j=1}^{N}\sum_{k=1}^{3} m_j c_j^k(t) \quad \mathbf{2}$$

where $c_j^k(t)$ is the velocity autocorrelation of atom j in the k direction

$$c_j^k(t) = \lim_{\tau-\infty} \frac{\int_{-\tau}^{\tau} v_j^k(t'+t)v_j^k(t')\mathrm{d}t'}{\int_{-\tau}^{\tau}\mathrm{d}t'} = \lim_{\tau-\infty}\frac{1}{2\tau}\int_{-\tau}^{\tau} v_j^k(t'+t)v_j^k(t')\mathrm{d}t'$$

$v_j^k(t)$ is the velocity of the atom j in the k-th direction at time t. The atomic spectrum density $s_j^k(\upsilon)$ is simply the Fourier transform of $c_j^k(t)$ and is given by

$$s_j^k(\upsilon) = \lim_{\tau-\infty}\frac{1}{2\tau}\left|\int_{-\tau}^{\tau} v_j^k(t)\mathrm{e}^{-i2\pi\upsilon t}\mathrm{d}t\right|^2 = \lim_{\tau-\infty}\frac{1}{2\tau}\int_{-\tau}^{\tau}\int_{-\tau}^{\tau} v_j^k(t)v_j^k(t+t')\mathrm{d}t'\mathrm{e}^{-i2\pi\upsilon t}\mathrm{d}t = \lim_{\tau-\infty}\int_{-\tau}^{\tau} c_j^k(t)\mathrm{e}^{-i2\pi\upsilon t}\mathrm{d}t \quad \mathbf{3}$$

From which we determined the vibrational DoS (power spectrum) as

$$S(\upsilon) = \frac{2}{kT}\sum_{j=1}^{N}\sum_{k=1}^{3} m_j s_j^k(\upsilon) \quad \mathbf{4}$$

where m_j is the mass of atom j.

RESULTS AND DISCUSSION

Differences in flexibility of the PX/JX motifs

Previous MD simulations have been reported on the crystal structure of B-DNA using explicit salt and water, validating the AMBER FF (20) and the PME method for calculating the non-bond forces (20–22,24). Simulations have also been performed in solution. The simulations on crystalline B-DNA lead to an overall calculated CRMSD for all atoms of 1.0–1.5 Å (20–22,24). This validates the accuracy of the FF. For the solution phase, there are no reliable experimental structures that can be compared with the simulations, which generally lead to RMSD differences of 3.6–4.2 Å from the crystal (22,24).

We carried out MD simulations for 2 ns in explicit salt and water for each of the five PX/JX nanostructures (PX65, JX1, JX2, JX3 and JX4) at 300 K. In each case, we defined the average MD structure by averaging the coordinates for various snapshots for the last 1 ns at an interval of 1 ps. This structure represents the time-averaged solution structure of the PX nanostructures (that one would compare to an NMR structure). These averaged structures for various PX structures are shown in Figure 3a and b. For JX2/JX3/JX4 (decreasing number of crossover points), we see that the two double helical domains move further apart, a feature highly undesirable for the application of these DNA motifs to construct periodic arrays. They move further apart and one helical domain gets twisted with respect to the second helical domain, leading to large writhing in the structure (see the side view in Figure 3b).

To obtain some idea about the stability as well as the flexibility of these structures, Figure 4a shows the time evolution of the CRMSD of instantaneous PX snapshots from *the initial minimized canonical structure*.

(i) For PX65, the CRMSD increases up to 400–500 ps and then stabilizes between 3 and 4 Å over the rest of the three ns trajectory.
(ii) On the other hand, for JX1, the CRMSD fluctuates between 3 and 4 Å up to 1 ns, but then increases to 5 Å over the next 1 ns.
(iii) For JX2/JX3, the CRMSD increases with time, going up to 8 Å in 2 ns, while for JX4 the CRMSD increases to 10 Å. These results suggest that the JX2, JX3 and JX4 structures will not retain their helical DNA structures and perhaps fall apart (but proving this would require much longer simulation times).

Experimentally it has not been possible to form any of these structures including PX65 in the presence of Na^+ (N. Seeman, personal communication). They have been formed only in the presence of Mg^{2+}. On the other hand, in our simulation we see that in the presence of Na^+, PX65 is a very stable molecule, and we suggest continued experimental studies in Na^+ to clarify the apparent disagreement between experiment and theory. We also plan to study these nanostructures in the presence of Mg^{2+} (Maiti,P.K., Pascal,T.A., Vaidehi,N. and Goddard,W.A.I., submitted). In addition to the comparison to the initial minimized structure, we also calculated the CRMSD of these nanostructures with respect to the time averaged solution structures as a function of time (see Figure 4b). This gives a better measure of the fluctuations in the structures. This CRMSD was calculated for the whole 2 ns MD runs. We see that the average solution structure for JX2, JX3 and JX4 deviates significantly from their average structure. To provide a quantitative measure of how the separation of the two helical domains varies as a function of the number of crossover points, Figure 5 shows the distance between the center of mass of the two helices during the dynamics. For PX65 the separation is ~20 Å, which is expected for such a structure; the diameter of normal B-DNA. As the number of crossover points decreases,

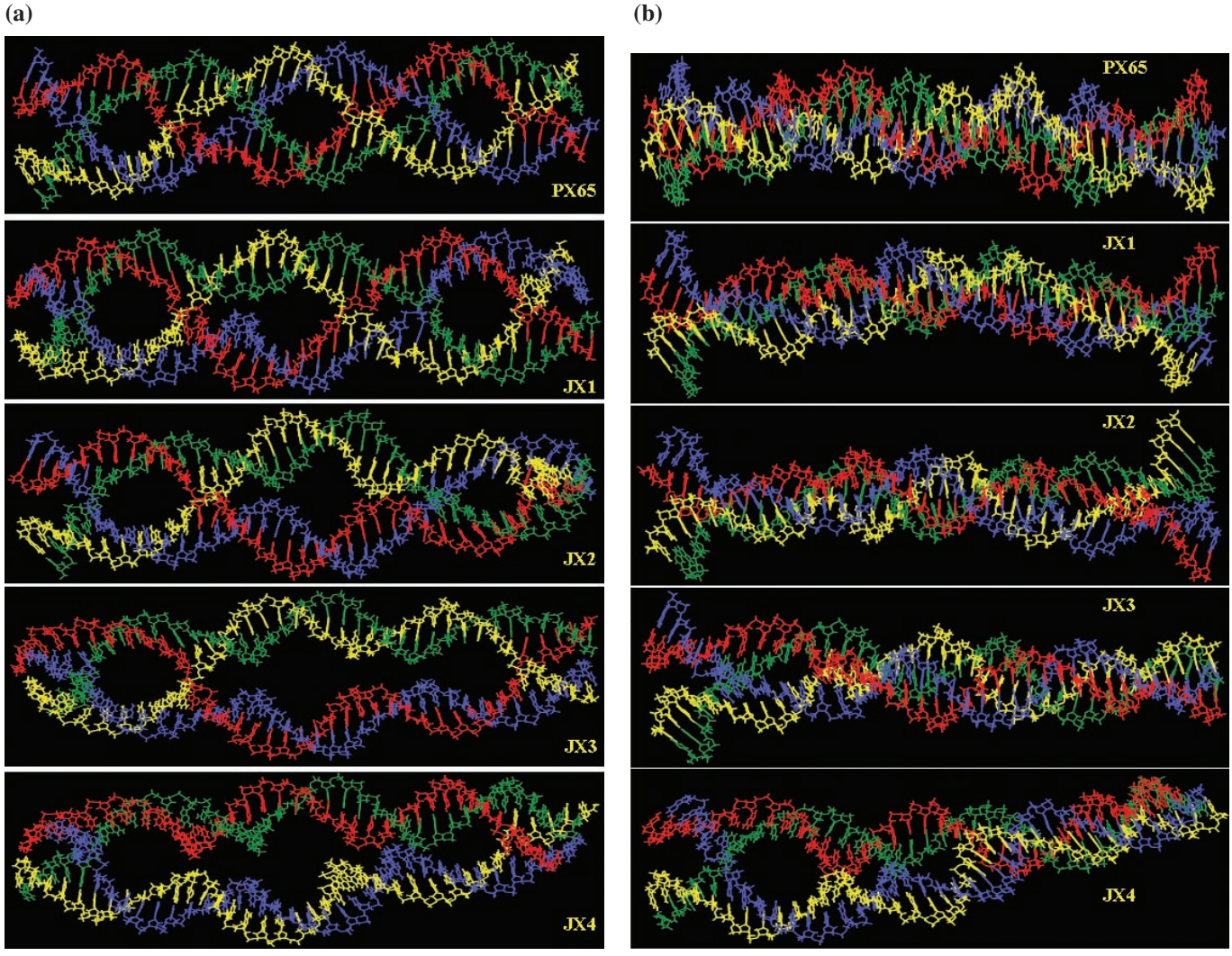

Figure 3. (**a**) Averaged dynamics structure for various PX molecules. Water molecules and counter ions are not shown for clarity. Note that with decreasing number of crossover points, the two double helical domains move further apart from each other. (**b**) Averaged dynamics structure for various PX molecules (side view). For clarity, water molecules and counter ions are not shown. With decreasing number of crossover points, there is significant bending of the two helical axis in the opposite direction leading to large writhing in the structure (see Table 4).

the separation increases reaching a maximum of 24 Å for JX3. Such increase in separation of the two helices as a function of the crossover separation has been found experimentally for DX molecules as well (30). Surprisingly, for JX4, we see a decrease in the separation to 22.5 Å. Very large difference in the bending angle of the two helical axes (~2° for PX65 and 40° for JX4) and resulting writhing in the structure (see Table 4) might be the reason behind this behavior.

Helicoidal parameters and groove dimensions for the PX/JX motifs

Table 2 provides details of the conformational helicoidal parameters of the PX/JX structures averaged over the last 400 ps of the 2 ns long dynamics. For comparison, we also give the values for the two double helices in their non-crossover form. Most helicoidal parameters for the two helices in the PX/JX structures have average values very similar to the corresponding B-DNA form. For example, the average helical twist for all the PX/JX structures fluctuates between 30 and 32°, the range expected for normal B-DNA. This indicates that even though the two helical domains of the crossover structures move further apart as the number of crossover points decreases, the individual double helix regions preserve their B-DNA form. However, the presence of the crossovers points influences the helical conformation significantly. Figure 6 shows the values of rise, tilt, roll and twist averaged over the MD as a function of the sequence along the backbone. At or near the crossover points, we see very large variations in these parameters from the values expected for a B-DNA (denoted by horizontal solid lines in Figure 6). Also for various JX motifs, we see similar trends: the values for rise, tilt, roll and twist for the individual helices remain close to the values expected for normal B-DNA. Table 3 compares the major and minor groove width of the PX/JX structures with the normal B-DNA of same length and sequence. We see that for PX65 and JX1 minor groove width narrows by 10% (from 6.95 to 6.3 Å) while major groove depth narrows by 47%

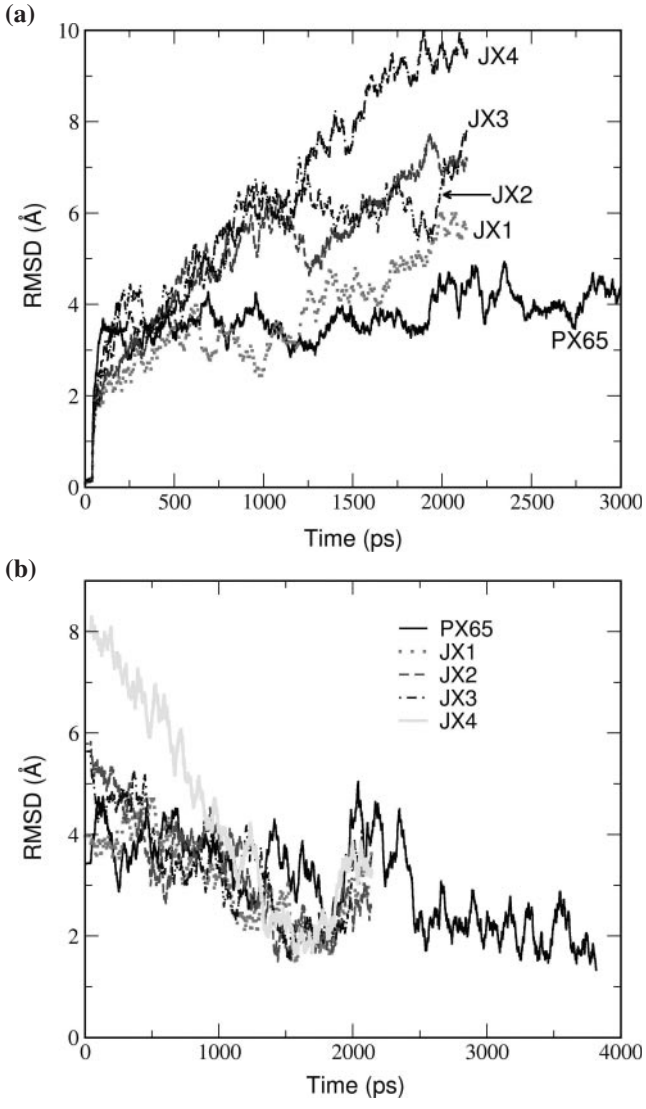

Figure 4. (**a**) Variation of the CRMSD of all atoms of various snapshots from the MD simulation run with respect to the starting minimized canonical structures. (**b**) RMSD with respect to average dynamics structure for different PX/JX molecules. The averaged structures were generated by averaging the coordinates for the last 1 ns of the 2 ns long MD runs. PX65/JX1 with CRMSD 3–5 Å is a stable molecule. Large CRMSD for JX2, JX3 and JX4 (8–10 Å) suggests that these structures will not retain their helical DNA structures and perhaps fall apart.

(from 7.9 to 4.2 Å) compared with its normal B-DNA counterpart. However, for JX2, JX3 and JX4, the minor groove width and depth approaches the canonical B-DNA value, while there is slight increase in the major groove width. These changes might affect the binding of various regulatory proteins to these crossover structures and might be used to physically separate the various generations of crossover structures.

End-to-end distances, strand shortening and bending of helical axis

The variation of end-to-end distance as a function of the number of crossover points is a measure of rigidity for the

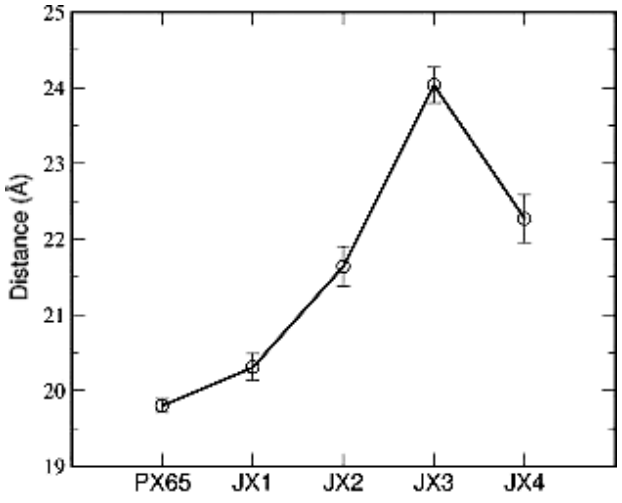

Figure 5. Distance between the center of mass of the two helices. With decreasing number of crossover points, the two helices move apart. The lowering of the distance for JX4 might be due to the large writhing during dynamics. The data has been averaged over the last 400 ps of the 2 ns long dynamics.

crossover molecules. Another closely related quantity is the variation of 'strand shortening' for various PX/JX structures over the dynamics. End-to-end distance and strand shortening are calculated as follows: CURVE algorithm outputs the vectorial direction of each local helical axis segment U and its reference point P. The path length between successive helical axis reference points is calculated as

$$\text{path} = \sum |\vec{P}_i - \vec{P}_{i-1}|$$

and the end-to-end distance of the DNA fragment is calculated as

$$R_e = |\vec{P}_1 - \vec{P}_N|$$

where $\vec{P}_1$ and $\vec{P}_N$ are the reference points for the two end helical axis corresponding to two terminal nucleotides. The difference between the sum of all the path lengths and the total end-to-end distance is a measure of the strand shortening. Table 5 reports the average end-to-end distance and strand shortening for both helices over last 200–400 ps of the 2 ns long dynamics.

We see that PX65 has the largest end-to-end extension (126 Å for helix1 and 128 Å for helix2) and smallest strand shortening (6.24 Å for helix1 and 5.05 Å for helix2). On the other hand, JX4 shows the smallest end-to-end extensions (116 Å for helix1 and 119 Å for helix2) and the large strand shortening (12.3 Å for helix1 and 9.8 Å for helix2). This is consistent with the writhing observed for JX4. The general increase in the end-to-end extension and decrease in strand shortening with increasing number of crossover points implies that increased number of crossover points induces enhanced rigidity in these molecules. This is also observed in the vibrational mode analysis presented in Normal mode analysis section. The larger strand shortening is accompanied by the significant bending in the DNA helical structure, as seen in Table 4.

Table 2. Helicoidal parameters for the PX/JX molecules averaged over the last 400 ps of the 2 ns MD runs

Parameter	B-DNA		PX65		JX1	
	Helix1	Helix2	Helix1	Helix2	Helix1	Helix2
Shift (Å)	0.00 (0.3)	−0.01 (0.5)	−0.02 (0.7)	0.00 (0.8)	−0.03 (0.6)	−0.01 (0.5)
Slide (Å)	−0.15 (0.3)	−0.15 (0.3)	−0.05 (0.8)	−0.07 (0.7)	−0.10 (0.4)	−0.12 (0.4)
Rise (Å)	3.39 (0.4)	3.39 (0.4)	3.53 (0.6)	3.57 (0.4)	3.47 (0.4)	3.48 (0.4)
Tilt (degrees)	0.27 (3.4)	−0.17 (2.1)	−0.25 (5.0)	0.64 (4.3)	0.07 (3.4)	−0.03 (4.3)
Roll (degrees)	6.37 (5.9)	6.16 (8.1)	2.08 (9.8)	3.34 (11.9)	4.75 (9.2)	4.30 (12.6)
Twist (degrees)	29.71 (3.7)	30.46 (4.5)	32.10 (5.3)	31.7 (7.4)	32.49 (4.9)	32.18 (6.6)

Parameter	JX2		JX3		JX4	
	Helix1	Helix2	Helix1	Helix2	Helix1	Helix2
Shift (Å)	−0.02 (0.6)	0.01 (0.5)	−0.01 (0.5)	−0.03 (0.4)	0.05 (1.0)	0.01 (0.4)
Slide (Å)	−0.12 (0.4)	−0.13 (0.4)	−0.09 (0.5)	−0.08 (0.6)	−0.10 (0.6)	−0.09 (0.5)
Rise (Å)	3.48 (0.5)	3.47 (0.5)	3.48 (0.5)	3.49 (0.5)	3.5 (0.4)	3.40 (0.3)
Tilt (degrees)	−0.26 (3.5)	−0.33 (3.3)	0.05 (3.3)	0.12 (3.2)	−2.8 (6.2)	−0.04 (3.1)
Roll (degrees)	5.11 (8.4)	5.50 (10.3)	4.78 (8.9)	4.26 (12.5)	4.30 (12.1)	3.90 (9.7)
Twist (degrees)	32.3 (5.4)	31.85 (5.7)	31.58 (5.5)	31.94 (6.0)	30.70 (7.8)	32.39 (6.9)

Here, the PX/JX molecules are analyzed in terms of its two double helices. For comparison, we have also tabulated the helical parameters for normal B-DNA of same length and sequence. The RMS deviation from the MD is shown in parenthesis. Note that the individual double helices of the crossover structure retain their B-DNA form quite well.

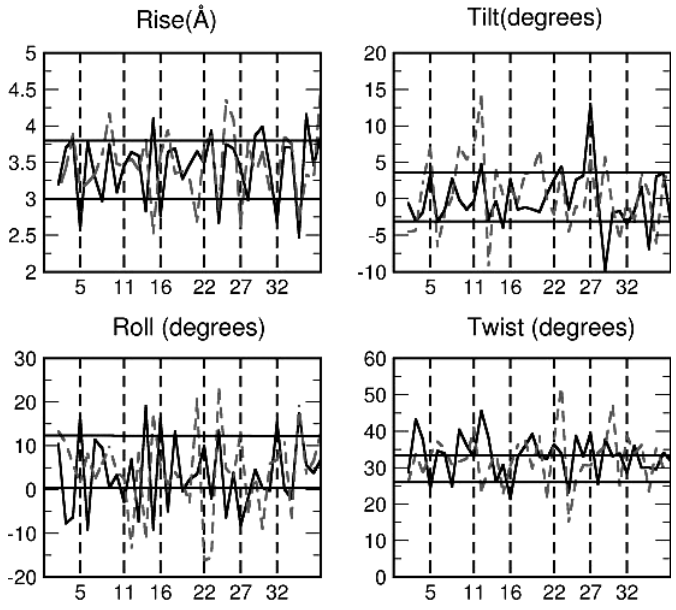

Figure 6. Average rise, tilt, roll and twist for PX motif. Solid line is for helix1 and broken line is for helix2. The vertical lines correspond to the crossover points. The horizontal solid lines give the upper bound and lower bound for the corresponding quantities expected for the helices in their B-DNA form (non-crossover form) during the dynamics. The data has been averaged over last 400 ps of the 3 ns long dynamics. In general, the two double helical domains in the crossover structure keep their B-DNA form quite well. However, at or near crossover points the helical parameters deviate significantly from the values expected in their B-DNA form.

Table 3. Average major groove and minor groove width for all the PX/JX molecules

Molecules	Major groove width (Å)	Minor groove width (Å)	Major groove depth (Å)	Minor groove depth (Å)
B-DNA				
Helix1	13.65 (0.4)	6.79 (0.2)	7.32 (0.4)	4.11 (0.7)
Helix2	14.53 (0.4)	7.1 (0.2)	8.43 (0.3)	3.81 (0.1)
PX65				
Helix1	13.93 (0.3)	6.43 (0.2)	4.52 (0.3)	4.66 (0.2)
Helix2	13.94 (0.3)	6.27 (0.3)	3.82 (0.3)	4.91 (0.1)
JX1				
Helix1	14.61 (0.2)	5.98 (0.2)	4.93 (0.3)	4.78 (0.1)
Helix2	14.94 (0.3)	6.16 (0.2)	5.26 (0.3)	4.53 (0.1)
JX2				
Helix1	14.75 (0.3)	6.25 (0.2)	7.03 (0.4)	4.27 (0.1)
Helix2	14.84 (0.5)	5.96 (0.3)	6.29 (0.3)	4.33 (0.2)
JX3				
Helix1	14.55 (0.2)	6.42 (0.1)	5.20 (0.3)	4.43 (0.1)
Helix2	14.06 (0.2)	5.99 (0.2)	4.92 (0.3)	4.72 (0.1)
JX4				
Helix1	14.22 (0.3)	6.67 (0.3)	6.68 (0.3)	4.18 (0.1)
Helix2	14.42 (0.3)	6.54 (0.2)	6.72 (0.6)	4.19 (0.2)

The data has been averaged over the last 400 ps of the 2.5 ns long MD runs. The width and depths are the sequence averaged values computed with program Curves (32). We see narrowing of minor groove width and major groove depth for PX65/JX1 compared to its normal B-DNA counterpart. However, as the number of crossover points decreases, for JX2/JX3/JX4, the minor groove width and depth approaches the canonical B-DNA value.

This increased bending with decreased crossovers is further confirmed by the changes in the bending angle of each double helix in every PX/JX structure. The bending angle is calculated as the angle between the successive $\vec{U}_i$ vector and is defined as

$$\theta = \cos^{-1}\left(\vec{U}_i \bullet \vec{U}_{i+1}\right)$$

Figure 7 shows the bending angle variation for *i*-th and (*i* + 5)-th base pair calculated for the two double helices for various PX/JX nanostructures averaged over the MD simulations. There is no appreciable bending visible for PX65. However, increased bending occurs at or near each missing crossover point. Thus, for JX1, the missing crossover at the 16th nucleotide position leads bending at or near this crossover point that is 50% larger than the other parts of the structure. This increased bending is also evident in Figures 3, showing snapshots from the MD simulations for each PX structure.

Combining the effect of strand shortening with the bending, we infer that all JX structures show large writhing in solution

Table 4. Average global bend, global roll and tilt angle calculated by Madbend (31)

Molecules	Global bend (degrees)	Global tilt (degrees)	Global roll (degrees)
B-DNA			
Helix1	14.14 (8.3)	4.54 (9.1)	−1.78 (12.8)
Helix2	24.4 (14.2)	−14.14 (14.9)	14.1 (13.1)
PX65			
Helix1	39.01 (13.1)	−15.06 (13.4)	−33.68 (12.3)
Helix2	36.68 (12.3)	2.41 (12.2)	−34.28 (12.9)
JX1			
Helix1	22.75 (11.59)	14.84 (11.2)	−8.07 (15.5)
Helix2	36.41 (10.87)	−17.84(11.7)	−29.08 (11.9)
JX2			
Helix1	15.53 (8.9)	5.75 (11.2)	−3.27 (12.3)
Helix2	35.06 (10.7)	17.86 (19.2)	−20.43 (15.5)
JX3			
Helix1	27.62 (10.6)	−24.22 (10.9)	8.0 (10.3)
Helix2	59.09 (14.1)	−34.11 (11.1)	−45.83 (17.4)
JX4			
Helix1	71.74 (10.5)	−69.28 (12.0)	−8.0 (15.8)
Helix2	32.58 (13.1)	12.42 (10.1)	−27.98 (13.9)

The data has been averaged over last 400 ps of the 2 ns long MD runs. The SDs are shown in brackets. Bends in the helical axis defined by a negative roll angle indicate bending toward the minor groove, while bends defined by a positive roll angle correspond to bending toward the major groove (31). For PX65/JX1, similar bend angle in the same direction (toward minor groove) might be the reason for their greater stability. On the other hand, for JX2 and JX4, we see that the two helices have very different bend angle either in the same direction or in the opposite direction. This led to the very high strain in the all the JX structures as is evident from our strain energy calculation.

Table 5. End-to-end distance and strand shortening for PX/JX molecules

Molecules	End-to-end distance (Å)		Strand shortening (Å)	
	Helix1	Helix2	Helix1	Helix2
B-DNA	119.31 (1.0)	117.54 (1.33)	6.89 (1.16)	8.79 (1.77)
PX65	126.10 (1.36)	128.48 (1.64)	6.24 (0.97)	5.05 (0.96)
JX1	123.75 (1.03)	124.25 (1.09)	7.51 (0.88)	7.23 (1.36)
JX2	122.03 (0.92)	118.26 (0.88)	8.76 (1.34)	11.82 (2.15)
JX3	124.42 (0.97)	123.73 (1.17)	6.29 (0.79)	8.47 (1.28)
JX4	115.89 (1.35)	118.98 (0.86)	12.30 (0.89)	9.75 (1.25)

The data has been averaged over last 200–400 ps of the 2.1 ns long dynamics. The SDs are shown in brackets. B-DNA helix1 and helix2 corresponds to the case when the simulation has been performed with the B-DNA with 38 bp with the same sequence for the two double helical domain as shown in Figure 1. We see increase in end-to-end extension and decrease in strand shortening with increasing number of crossover points. These imply that higher number of crossover points induce enhanced rigidity to these molecules.

compared with the PX65 structure. This writhing is an important structural feature to be taken into account in designing nanostructures. For example, the minimal writhing in PX65 makes it a better choice than any JX structures for constructing 2D arrays using crossover nanostructures. Figure 3b compares the side views (the average solution structure from the MD run) of the solution structure for PX65 with various JX structures. Clearly, JX2, JX3 and JX4 bend much more than PX65.

We also calculated the global helical bending for each of the two helices using the algorithm developed by Strahs and Schlick (31). This method computes the DNA curvature by summing the projected components of local base pair step tilt and roll angles after adjusting the helical twist. Our analysis for the global angles is based on the values of local tilt and roll angles for each base pair step computed by the Curves program (32). Bends in the helical axis defined by a negative roll angle indicate bending toward the minor groove, while bends defined by a positive roll angle correspond to bending toward the major groove (31). Table 4 gives the values of global bend, tilt and roll for the two helices for all the PX/JX molecules studied in this paper. For comparison, we also calculated the values for the helix1 and helix2 in their B-DNA form. The similar bend angle in the same direction (toward minor groove) observed for PX65, JX1 and B-DNA is consistent with their greater stability. On the other hand, for JX2 and JX4, we see that the two helices have very different bend angles sometimes in the same direction and sometimes in the opposite direction. This leads to the very high strain in the all JX structures found in our strain energy calculation.

Strain energy

As a reference for calculating the strain energy, we carried out MD simulations on the two separate double helices with the same sequence as the PX/JX structures (given in Figure 1). These explicit solvent simulations are used to extract the strain energy for just the DNA fragment and serves as our reference energy. Earlier (Maiti,P.K., Pascal,T.A., Vaidehi,N., Heo,J. and Goddard,W.A.I., submitted), we used the ANAL module of the AMBER7 (18) to obtain the energy for just the DNA. However, ANAL uses evaluate the energetic assuming a non-periodic structure with real space cut-offs in computing non-bond interactions, rather than the full periodic calculation using PME that was used in the dynamics. The result is a very inaccurate estimate of the electrostatics interactions. Now, we obtain the DNA energy from the explicit solvent runs using the MPSIM program (33), which uses the PME method for the non-bond coulomb interactions. The strain energy is calculated as described in Methods and plotted in Figure 8. We see that PX and JX1 have very little strain, indicating that they are very stable. On the other hand, the very high strains for JX2, JX3 and JX4 suggest that these molecules are very unstable. This indicates that increased number of crossover points increases stability. As the number of crossovers increases, these molecules become quite rigid, an essential feature for their use as building blocks for constructing such larger supramolecular aggregates as 2D or 3D arrays.

Normal mode analysis of the PX/JX structures

The density and distribution of vibrational states at low frequencies provides valuable insight into the structural changes induced by the crossover points. Accordingly, we calculated the distribution of vibrational modes for each PX/JX structure using the analysis of velocity autocorrelation function, as described in Methods. The vibrational (power) spectra for all crossover structures are shown in Figure 9. For comparison, we also show the vibrational spectrum for one double helix corresponding to the crossover structures.

The high frequency regime leads to quite similar vibrational spectra for all the PX/JX motifs. Since the AMBER FF requires use of the SHAKE algorithm to constrain the high frequency XH bond vibrations, we do not find any mode frequencies beyond 1400 cm^{-1}.

For frequencies below 100 cm^{-1}, we see that the DoS decreases with increased number of crossover points.

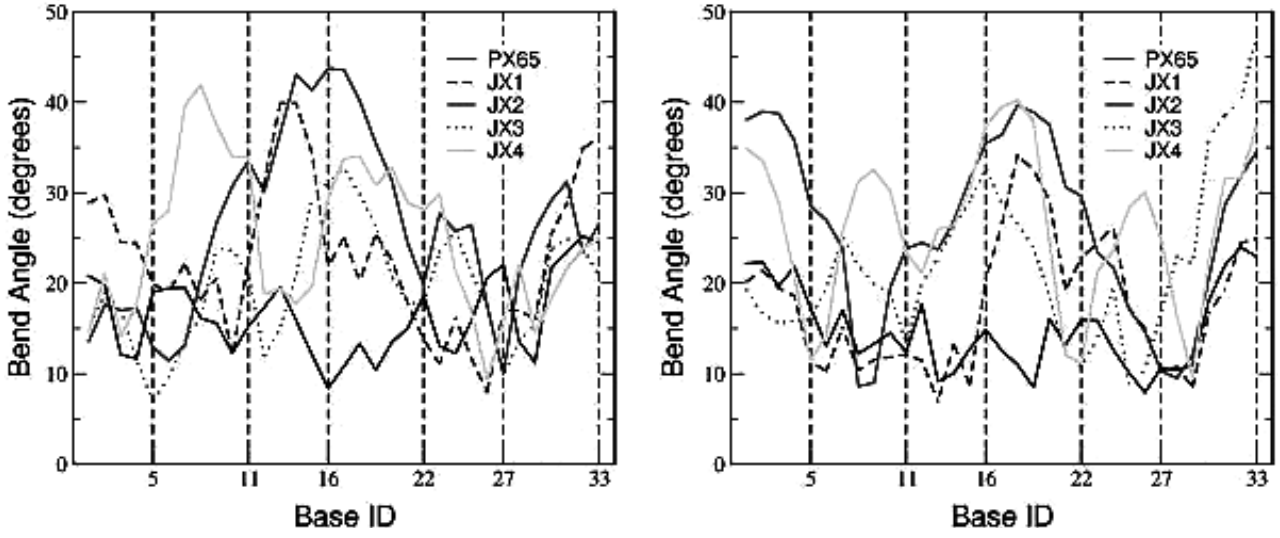

Figure 7. Bending angle between every i-th and $(i+5)$-th nucleotide for (**a**) helix1 and (**b**) helix2 for each of the PX/JX structures. There is no appreciable bending visible for PX65. However, with decreasing number of crossover points, increased bending occurs at or near each missing crossover point.

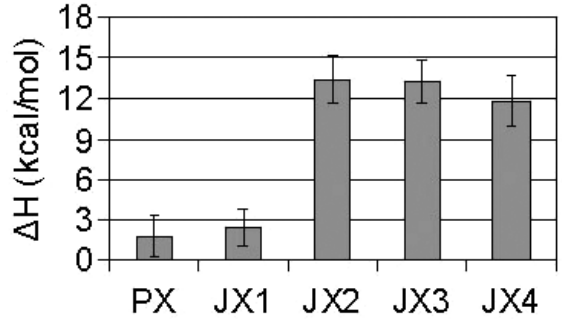

Figure 8. Strain energy for various PX/JX structures. The starin energy has been calculated with respect to the two separate double helices. Very little strain energy (~3 kcal/mol/bp) for PX65/JX1 indicates that they are very stable. On the other hand the very high strains for JX2, JX3, and JX4 suggest that these molecules are very unstable.

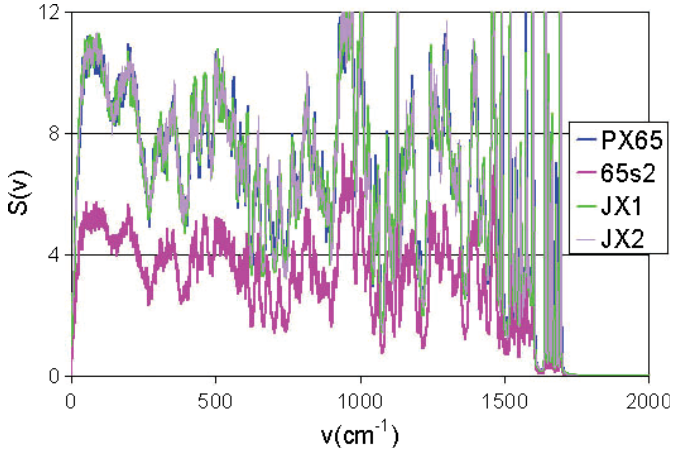

Figure 9. Power spectrum for various PXJX crossover molecules. For comparison, we have also shown the spectrum from 65S2, which is a B-DNA with same length and sequence as that of one of the double helix of PX65.

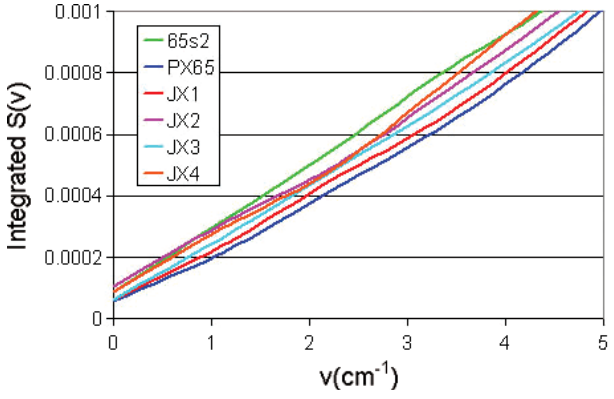

Figure 10. Intgrated DoS S(ν) as a function of ν (cm^{-1}) for various PX/JX crossover molecules. The population of low frequency modes gradually decreases as the number of crossover points increases making PX65 (with most number of crossover points) more rigid than the other JX structures.

Integrating the power spectrum leads to the integrated DoS shown in Figure 10 for all the PX/JX molecules. The population of low frequency modes is a direct measurement of the rigidity of the DNA molecules since they dominate the overall global dynamics. Thus, the population of low frequency modes gradually decreases as the number of crossover points increases. This indicates the enhanced rigidity of the crossover molecules with increased number of crossover points. This observation is consistent with the experimental findings on another class of crossover molecules, namely the DX molecules (34), which were found to be very rigid compared with linear DNA molecules. Among all the motifs studied here, PX65 turns out to be more rigid than other structures.

SUMMARY AND CONCLUSIONS

These fully atomistic studies on PX65 and its JXM ($M = 1, 2, 3$ and 4) topoisomers clearly demonstrate that increased number

of crossover points provides increased stability to the crossover motifs. However, for the Na^+ monovalent ions used in this study, the JX motifs are not able to maintain the parallel double helix crossover structures. Thus, the two helical domains of the crossover structure move increasingly far apart with decreasing number of crossover points. This leads to very large deviations [CRMSD (~10 Å)] of the JX2, JX3 and JX4 motifs from their initial canonical structures. Our strain energy calculations show that motifs with fewer crossover points have strain energies in the range of ~12–14 kcal/mol/bp, compared with ~3 kcal/mol/bp for PX65 with largest number of crossover points. Our results are consistent with experimental observations that stable JX motifs are found only when using divalent Mg^{2+} ions. It is plausible that Mg^{2+} ions might induce effective attraction between the two helical domains to maintain their crossover structures, and we plan to study the behavior of PX/JX motifs in the presence of divalent Mg ions.

ACKNOWLEDGEMENTS

We thank Prof. Nadrian Seeman (New York University) for suggesting these calculations and for a great deal of advice and sharing of experimental data prior to publication. We also thank Mr Gene Carter (author of Namot2) for collaborating with us in making changes to the code to facilitate building of PX crossover points. We also thank Dr Shiang-Tai Lin for help in doing the vibrational DoS analysis. Also, we thank Prof. Erik Winfree for useful discussions. This research was supported by NSF grants under NIRT-CTS-0103002. The MSC facilities used in these studies were funded by grants from ARO (DURIP), ONR (DURIP), NSF (MRI) and IBM (SUR). The MSC is also supported by grants from NIH, NSF, DOE, Chevron-Texaco, General Motors, Seiko Epson, Asahi Kasei and Beckman Institute.

REFERENCES

1. Seeman,N.C. (2003) DNA in a material world. *Nature*, **421**, 427–431.
2. Seeman,N.C. (2003) Biochemistry and structural DNA nanotechnology: an evolving symbiotic relationship. *Biochemistry*, **42**, 7259–7269.
3. Winfree,E., Liu,F.R., Wenzler,L.A. and Seeman,N.C. (1998) Design and self-assembly of two-dimensional DNA crystals. *Nature*, **394**, 539–544.
4. Seeman,N.C., Liu,F.R., Mao,C.D., Yang,X.P., Wenzler,L.A., Sha,R.J., Sun,W.Q., Shen,Z.Y., Li,X.J., Qi,J., Zhang,Y.W., Fu,T.J., Chen,J.H. and Winfree,E. (2000) Two dimensions and two states in DNA nanotechnology. *J. Biomol. Struct. Dyn.*, 253–262.
5. Seeman,N.C., Liu,F., Wenzler,L.A. and Winfree,E. (1999) Design and modification of two dimensional DNA arrays. *Biophys. J.*, **76**, A152–A152.
6. LaBean,T.H., Yan,H., Kopatsch,J., Liu,F.R., Winfree,E., Reif,J.H. and Seeman,N.C. (2000) Construction, analysis, ligation, and self-assembly of DNA triple crossover complexes. *J. Am. Chem. Soc.*, **122**, 1848–1860.
7. Adleman,L.M. (1994) Molecular computation of solutions to combinatorial problems. *Science*, **266**, 1021–1024.
8. Winfree,E. (1995) In Lipton,R.J. and Baum,B.E. (eds), *DNA Based Computers: Proceedings of a DIMACS Workshop, April 4*, American Mathematical Society, Providence, pp. 199–221.
9. Liu,Q.H., Wang,L.M., Frutos,A.G., Condon,A.E., Corn,R.M. and Smith,L.M. (2000) DNA computing on surfaces. *Nature*, **403**, 175–179.
10. Yan,H., Park,S.H., Finkelstein,G., Reif,J.H. and LaBean,T.H. (2003) DNA-templated self-assembly of protein arrays and highly conductive nanowires. *Science*, **301**, 1882–1884.
11. Mao,C.D., Sun,W.Q., Shen,Z.Y. and Seeman,N.C. (1999) A nanomechanical device based on the B-Z transition of DNA. *Nature*, **397**, 144–146.
12. Yurke,B., Turberfield,A.J., Mills,A.P., Simmel,F.C. and Neumann,J.L. (2000) A DNA-fuelled molecular machine made of DNA. *Nature*, **406**, 605–608.
13. Alberti,P. and Mergny,J.L. (2003) DNA duplex-quadruplex exchange as the basis for a nanomolecular machine. *Proc. Natl Acad. Sci. USA*, **100**, 1569–1573.
14. Seeman,N.C. (2001) DNA nicks and nodes and nanotechnology. *Nano Lett.*, **1**, 22–26.
15. Yan,H., Zhang,X.P., Shen,Z.Y. and Seeman,N.C. (2002) A robust DNA mechanical device controlled by hybridization topology. *Nature*, **415**, 62–65.
16. Shen,Z.Y., Yan,H., Wang,T. and Seeman,N.C. (2004) Paranemic crossover DNA: a generalized Holliday structure with applications in nanotechnology. *J. Am. Chem. Soc.*, **126**, 1666–1674.
17. Tung,C.S. and Carter,E.S. (1994) Nucleic acid modeling tool (NAMOT): an interactive graphic tool for modeling nucleic acid structures. *Comput. Appl. Biosci.*, **10**, 427–433.
18. Case,D.A., Pearlman,D.A., Caldwell,J.W., Cheatham,T.E., Wang,J., Ross,W.S., Simmerling,C., Darden,T., Merz,K.M., Stanton,R.V. *et al.* (1999) AMBER 7 edit. University of California, San Francisco.
19. Cornell,W.D., Cieplak,P., Bayly,C.I., Gould,I.R., Merz,K.M., Ferguson,D.M., Spellmeyer,D.C., Fox,T., Caldwell,J.W. and Kollman,P.A. (1995) A second generation force field for the simulation of proteins, nucleic acids, and organic molecules. *J. Am. Chem. Soc.*, **117**, 5179–5197.
20. Lee,H., Darden,T. and Pedersen,L. (1995) Accurate crystal molecular-dynamics simulations using particle—Mesh-Ewald—RNA dinucleotides—Apu and Gpc. *Chem. Phys. Lett.*, **243**, 229–235.
21. York,D.M., Yang,W.T., Lee,H., Darden,T. and Pedersen,L.G. (1995) Toward the accurate modeling of DNA—the importance of long-range electrostatics. *J. Am. Chem. Soc.*, **117**, 5001–5002.
22. Miaskiewicz,K., Miller,J., Cooney,M. and Osman,R. (1996) Computational simulations of DNA distortions by a cis,syn-cyclobutane thymine dimer lesion. *J. Am. Chem. Soc.*, **118**, 9156–9163.
23. Feig,M. and Pettitt,B.M. (1998) Structural equilibrium of DNA represented with different force fields. *Biophys. J.*, **75**, 134–149.
24. Bevan,D.R., Li,L.P., Pedersen,L.G. and Darden,T.A. (2000) Molecular dynamics simulations of the d(CCAACGTTGG)(2) decamer: influence of the crystal environment. *Biophys. J.*, **78**, 668–682.
25. Darden,T., York,D. and Pedersen,L. (1993) Particle Mesh Ewald—an *N*.Log(*N*) method for Ewald sums in large systems. *J. Chem. Phys.*, **98**, 10089–10092.
26. Essmann,U., Perera,L., Berkowitz,M.L., Darden,T., Lee,H. and Pedersen,L.G. (1995) A smooth particle mesh Ewald method. *J. Chem. Phys.*, **103**, 8577–8593.
27. Ryckaert,J.P., Ciccotti,G. and Berendsen,H.J.C. (1977) Numerical-integration of Cartesian equations of motion of a system with constraints—Molecular-dynamics of *N*-alkanes. *J. Comput. Phys.*, **23**, 327–341.
28. Berendsen,H.J.C., Postma,J.P.M., van Gunsteren,W.F., DiNola,A. and Haak,J.R. (1984) Berendesen thermostat. *J. Comput. Phys.*, **81**, 3684–3690.
29. Berens,P.H., Mackay,D.H.J., White,G.M. and Wilson,K.R. (1983) Thermodynamics and quantum corrections from molecular-dynamics for liquid water. *J. Chem. Phys.*, **79**, 2375–2389.
30. Fu,T.J. and Seeman,N.C. (1993) DNA double-crossover molecules. *Biochemistry*, **32**, 3211–3220.
31. Strahs,D. and Schlick,T. (2000) A-tract bending: insights into experimental structures by computational models. *J. Mol. Biol.*, **301**, 643–663.
32. Lavery,R. and Sklenar,H. (1988) The definition of generalized helicoidal parameters and of axis curvature for irregular nucleic acids. *J. Biomol. Struct. Dyn.*, **6**, 63–91.
33. Lim,K.T., Brunett,S., Iotov,M., McClurg,R.B., Vaidehi,N., Dasgupta,S., Taylor,S. and Goddard,W.A. (1997) Molecular dynamics for very large systems on massively parallel computers: the MPSim program. *J. Comput. Chem.*, **18**, 501–521.
34. Sa-Ardyen,P., Vologodskii,A.V. and Seeman,N.C. (2003) The flexibility of DNA double crossover molecules. *Biophys. J.*, **84**, 3829–3837.